

SIMULATION OF ENHANCED TURBULENT HEAT TRANSFER IN CORRUGATED WALL-CHANNELS

*M.K. Bassiouny**, *S.A. Wilson**, *S. Soliman*** and *Y. Rihan***

* The University of Menoufia, Faculty of Engineering, Mechanical Power Department, Shibin El-kom, Egypt

** Hot Laboratories Centre, Atomic Energy Authority, Egypt

ABSTRACT

A numerical study on hydrodynamic and heat transfer characteristics in a corrugated-wall short duct for turbulent flow is reported. The $k-\epsilon$ turbulence model with a refined near-wall model is adopted for the computation of the flow field for corrugation depth ratio ranging from 0.03 to 0.12 and pitch ratios of 1.8, 3 and 4.2. The Reynolds number considered in this study varies from 30000 to 150000. The proposed mathematical model is based mainly on the conservation equations of mass, momentum and energy. The strongly coupled set of differential equations are solved numerically together using the implicit scheme of finite volume method combining with an iterative procedure. The distribution of the local and average Nusselt number of air, pressure distribution along the wall, local shear stress coefficient and turbulent kinetic energy distribution are presented. Moreover, relative to a smooth duct, the enhancement of both local and global Nusselt number at different values of Reynolds numbers, depth and pitch ratios are documented in details. Comparisons between the present prediction and measurements of other authors show a good agreement. The results may be useful for gas turbine blade internal cooling or gas cooled nuclear reactors design.

Keywords: Numerical methods, corrugated ducts, turbulent flow, heat transfer.

INTRODUCTION

Gases are not good heat-transfer media, due to their very low density. However, they have been extensively used as coolants in reactors due to their low neutron absorption and low chemical activity. Much effort and ingenuity has been devoted to the improvement of the heat transfer in gas cooled reactors to increase the core power density and reduce the electrical power generating costs [1].

In the commercial gas cooled reactors this improvement has been achieved by means of extended heat-transfer surfaces (Magnox reactors) or by the so-called "artificial roughness" on the surface of the

fuel element rods (advanced gas-cooled reactors).

In the high temperature reactors even higher power densities are achieved by means of higher coolant pressures (up to 40-50 bar) and much higher fuel surface temperatures (up to 1000°C) made possible by the adoption of graphite as cladding and structural material.

Gas cooled reactors should have power densities in the core two orders of magnitude greater than those present in high temperature reactors [2]. Although a considerable part of this increase is due to the lack of moderator in the reactor, much higher heat-transfer coefficients are still required, especially because the fuel surface

temperatures, are considerably lower than in HTR's due to the use of metal, and not ceramic, cladding. This is achieved in part with higher gas pressures (pressures up to 80-130 bar have been proposed), in part again by the use of the artificial roughness. This artificial roughness acts as turbulence promoters breaking up the viscous sublayer in the fluid region nearest to the wall. Both the heat-transfer and the friction losses are increased [3].

In the modern turbine blade, heat transfer enhancement is accomplished by installing promoters, such as artificial roughness, on the two opposite walls of the internal cooling passages. Usually, the roughness elements are small ridges of a square cross section and are placed periodically at right angles to the main flow direction [4]. The cost paid for the higher heat transfer is an increase in the pressure drop. Turbine airfoil cooling designers would like to optimize the ridge geometry in order to obtain the best heat transfer coefficients for either a given coolant flow rate or an available pressure drop across the cooling passage.

Although quite a few work had appeared previously [5-10] the first important work on roughness was published by Nikuradse [11] in 1932. This and the subsequent work of Schlichting [12] were essentially performed to investigate the problem of the drag exerted by water on the hull of ships.

Among the first experimental investigations on heat transfer for flow inside artificially rough tubes we should like to mention those of Chu and Streeter [13] in 1949, Sams [14] and Nunner [15]. These data were given in terms of friction factors and Nusselt or Stanton numbers.

In 1963 Dipprey and Sabersky published experimental friction and heat-transfer data obtained for flow inside a tube with sand roughness surface [16]. Their method of correlating the heat-transfer results was similar to that used by Nikuradse [11] in correlating the friction data.

A number of friction and heat-transfer measurements on repeated-rib roughness in tube flow have been performed such as

Brouillette *et al.* [17] in 1957, Koch [18] in 1960, Molloy [19] in 1967, Gargaud and Paumard [20] in 1969 and Kalinin [21] in 1970. Webb, Eckert and Goldstein [22] carried out experiments on a tube with internal ribs. Their data covered a wide range of rib height to hydraulic diameter ratio, but only a pitch to height ratio greater than ten was used. Thereby, the ribs were normal to the main stream direction.

The effect of rib angle orientation on the local, regionally averaged heat transfer distributions and pressure drop in a square duct with two opposite ribbed walls were recently re-examined [23,24]. The results show that the "broken" V-shaped rib performs better than the angled rib [25].

The objective of the present study is to investigate theoretically the effect of corrugation on local heat transfer distribution and pressure drop in circular and rectangular channels. Thereby, the influence of Reynolds number and corrugation depth and pitch are taken into account. The theoretical results will then be compared with previous experimental data to check the validity and accuracy of the present mathematical model.

MATHEMATICAL MODEL

The mathematical model is based on solving the conservation equations of mass, momentum, and energy as well as the two equations of turbulence model (k-ε). The general form of the conservation equations can be given in the following form:

$$\frac{\partial}{\partial x} \left[\rho u \phi - \Gamma_{\phi} \frac{\partial \phi}{\partial x} \right] + \frac{\partial}{\partial y} \left[\rho v \phi - \Gamma_{\phi} \frac{\partial \phi}{\partial y} \right] = S_{\phi}$$

where ϕ is the dependent variable of the flow field, Γ_{ϕ} is the diffusion coefficient and S_{ϕ} is the source term. The quantities Γ_{ϕ} and S_{ϕ} are specific to a particular meaning of ϕ , as shown in Table 1.

The effective viscosity is the summation of the laminar and the turbulent eddy viscosity:

$$\mu_{\text{eff}} = \mu + \mu_t = \mu + C_{\mu} \rho k^2 / \epsilon$$

where, $C_{\mu} = 0.09$

The mathematical model is designed to investigate two cases: single as well as

double step domain. Figure 1 indicates the geometry of the two test cases considered.

Table 1 System of differential equations.

| ϕ | Γ_ϕ | S_ϕ | remarks |
|------------|-----------------------------|---|---------------------------|
| 1 | 0 | 0 | continuity |
| u | μ_{eff} | $-\partial p/\partial x + \partial/\partial y (\mu_{eff} \partial v/\partial x) + \partial/\partial x (\mu_{eff} \partial u/\partial x - 2/3(\mu_{eff} \cdot \nu u^*pk))$ | axial momentum |
| v | μ_{eff} | $-\partial p/\partial y + \partial/\partial y (\mu_{eff} \partial v/\partial y) - 2/3 (\mu_{eff} \cdot \nu u^*pk)$ | momentum in y-direction |
| i | μ_{eff}/σ_i | $-(u \partial p/\partial x + v \partial p/\partial y)$ | energy |
| k | μ_{eff}/σ_k | $\rho G - C_D \rho \epsilon$ | turbulence kinetic energy |
| ϵ | $\mu_{eff}/\sigma_\epsilon$ | $\frac{\epsilon}{K} K [\rho C_D G - C_D \rho \epsilon]$ | energy dissipation rate |

axis of symmetry, the normal derivatives of the flow parameters must vanish. The solid wall temperature is assumed to be constant along the wall, while the other flow parameters are taken equal to zero. The magnitude of each dependent variable (ϕ) in the grids near the wall is modified by using the standard wall functions [26, 27].

NUMERICAL SOLUTION

The relevant system of differential equations, given above, is solved via the finite volume method with an iterative procedure [28]. The grid system applied for this purpose is shown in Figure 2.

The iterative technique is continued until a convergent solution is reached. It was found that when the grid size is 22*22, the convergence occurs after 200 iterations with normalized residuals less than 0.005. The numerical computations are carried out under varying Reynolds number as well as the corrugation depth and pitch in both cases of circular and rectangular channels.

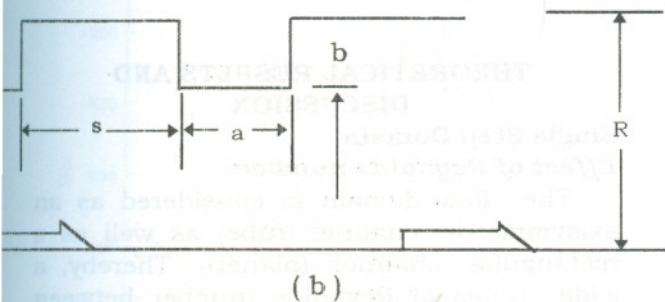
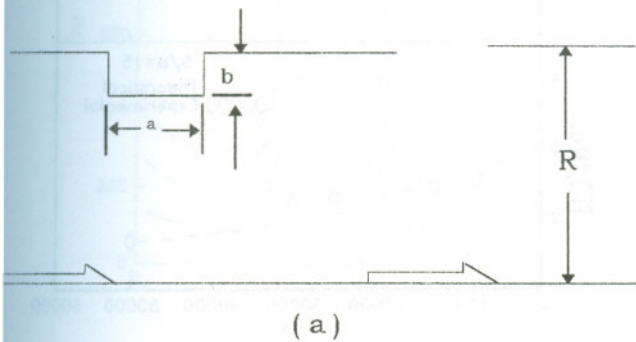


Figure 1 The geometry of the two test cases considered in the present work.

BOUNDARY CONDITIONS

The boundary conditions of the computational domain include the inlet conditions, the solid wall geometry and the axis of symmetry. At the entrance section the fluid is considered as one dimensional, turbulent and fully developed flow. At the

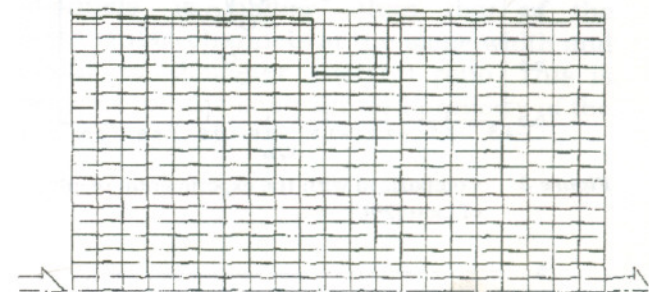


Figure 2 The grid system used in mathematical model.

COMPARISON WITH PUBLISHED EXPERIMENTAL DATA

In order to verify the validity of the present proposed mathematical model, a comparative study with previous experimental works of different researchers were performed. Thereby, the experimental data of Liou *et al.* [29] are compared with the theoretical results of the present model for data upstream and downstream the rib as indicated in Figure 3, for Re=12600 and S/b=7.2, and in Figure 4, for Re=13000 and S/b=10.

It is clear from the figures that when a confined flow passes over an internal rib, two reversed flow domains are established on both sides of the rib. The upstream reverse flow zone is less in size than that of the downstream. Therefore, the velocity gradients of the flow adjacent to the wall upstream the rib are much higher. This leads to an increase in the local heat transfer coefficient and consequently successive peaks in the local Nusselt number distribution curves are obtained on both sides of the ribbed wall. The upstream peak should be higher than the other.

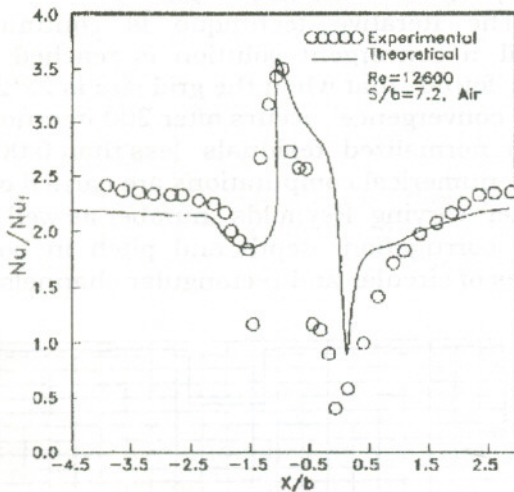


Figure 3 Comparison with the experimental results of Liou [29].

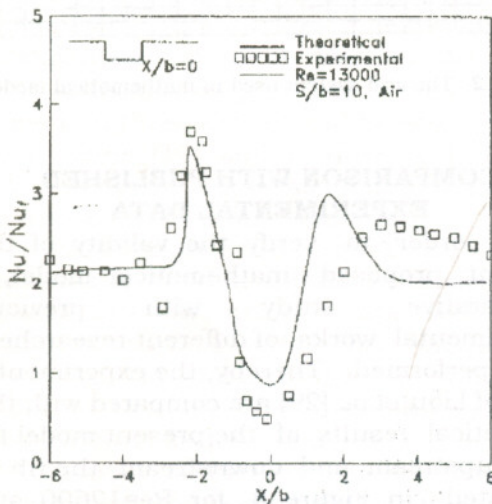


Figure 4 Local Nusselt number distribution for flow past a single rib in planer domain.

Figure 5 represents a comparison between the theoretical results and previously published experimental data [30] for the variation of the global Nusselt number against Reynolds number in case of $S/b = 10$ as well as 15. The comparisons show a fair agreement between both the computational and the experimental results.

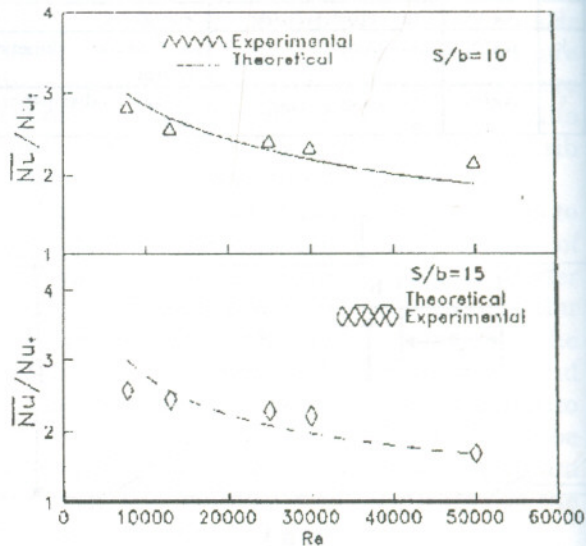


Figure 5 Effect of Reynolds number on the global Nusselt number.

THEORETICAL RESULTS AND DISCUSSION

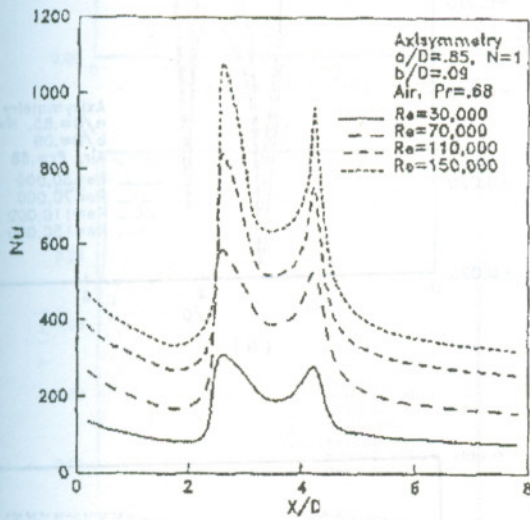
Single Step Domain

Effect of Reynolds number

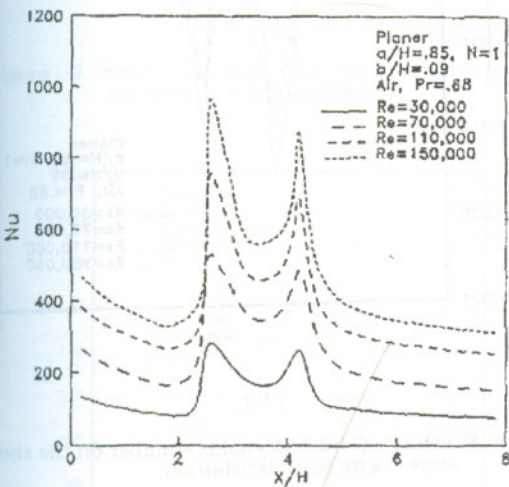
The flow domain is considered as an axisymmetric channel (tube) as well as a rectangular channel (planer). Thereby, a wide range of Reynolds number between 30,000 and 150,000 is applied to examine its effect on the local Nusselt number. The calculations are carried out for both the channel geometries considered (tubes and rectangular channels) with a corrugation width ratio of 0.85 and depth ratio of 0.09. The results indicate clearly the double peaks in Nusselt number distribution curves on both sides of the corrugation in case of axisymmetry, as seen in Figure 6-a and a rectangular channel, as seen in

Simulation of Enhanced Turbulent Heat Transfer in Corrugated Wall-Channels

Figure 6-b. This tendency is due to the reverse flow before and behind the corrugation. Increasing the inlet Reynolds number, the whole distribution of local Nusselt number increases. This returns to the increase of the amount of convective heat transfer from the wall with increasing the inlet fluid velocity.



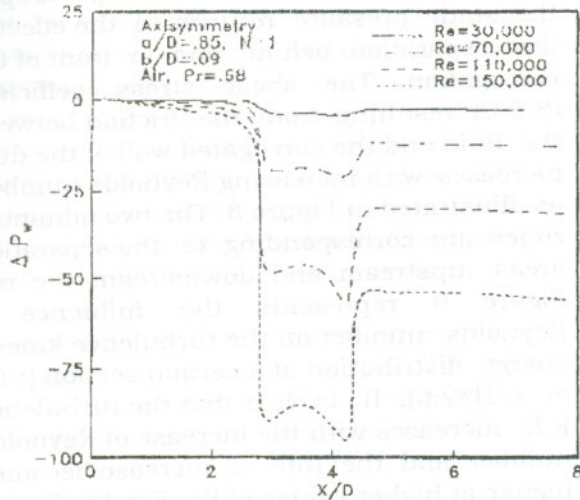
(a)



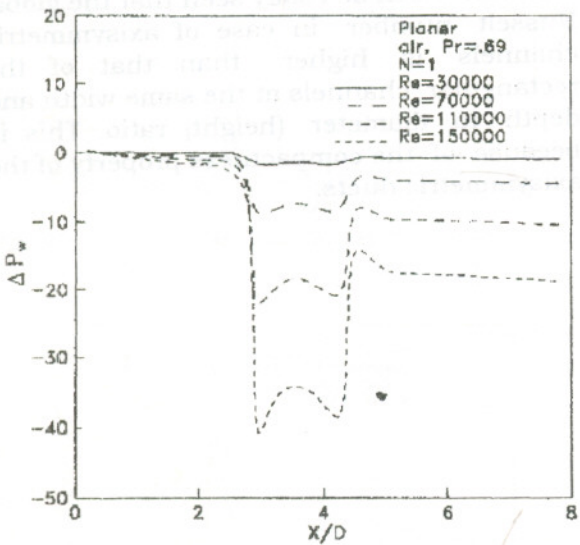
(b)

Figure 6 Effect of inlet Reynolds number on the local Nusselt distribution.

The static pressure along the wall is influenced directly by varying Reynolds number, as shown in Figure 7. Increasing the value of Reynolds number, the pressure recovery will decrease. The steep drop in the static pressure returns to the effect of flow separation behind and in front of the corrugation. The shear stress coefficient (S.S.C) resulting from the friction between the fluid and the corrugated wall of the duct increases with increasing Reynolds number, as illustrated in Figure 8. The two minimum zones are corresponding to the separation areas upstream and downstream the rib. Figure 9 represents the influence of Reynolds number on the turbulence kinetic energy distribution at a certain section (x/D or $x/H=2.6$). It is clear that the turbulence K.E increases with the increase of Reynolds number and the rate of increase becomes higher at higher values of Re. Finally, Figure 10 illustrates the steeply increase of the global Nusselt number with Reynolds number. It can be easily seen that the global Nusselt number in case of axisymmetric channels is higher than that of the rectangular channels at the same width and depth to diameter (height) ratio. This is because of the compactness property of the axisymmetric ducts.

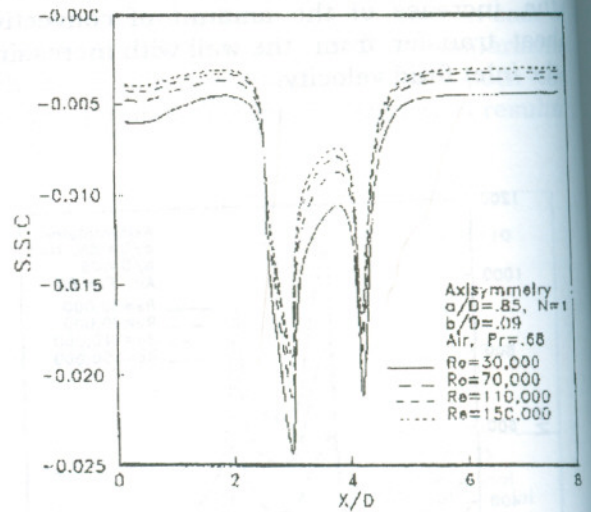


(a)

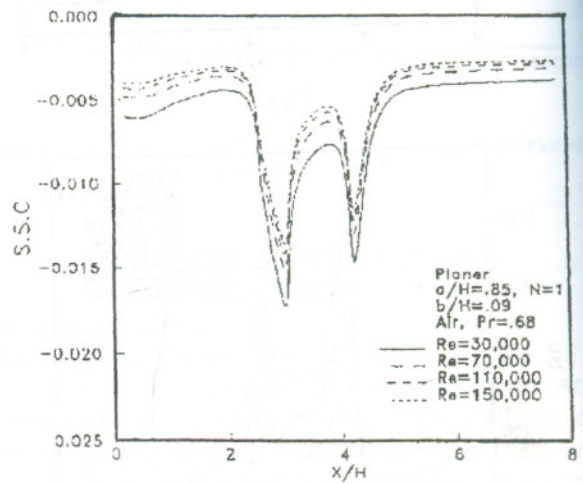


(b)

Figure 7 Effect of inlet Reynolds number on the pressure distribution at the wall.

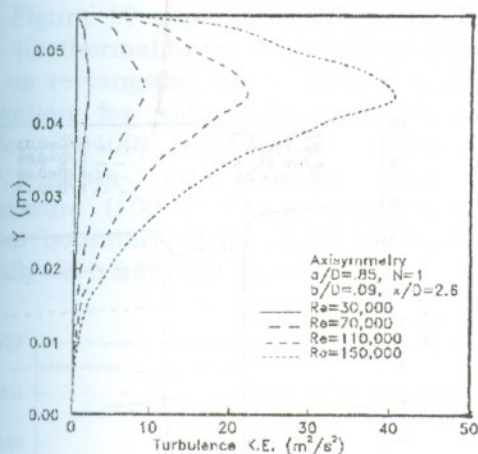


(a)

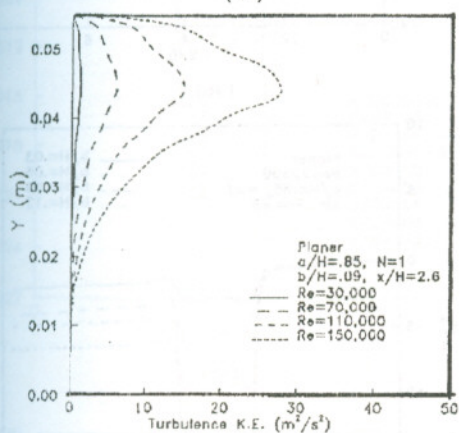


(b)

Figure 8 Effect of inlet Reynolds number on the shear stress coefficient distribution.



(a)



(b)

Figure 9 Effect of inlet Reynolds number on the turbulence K.E. distribution.

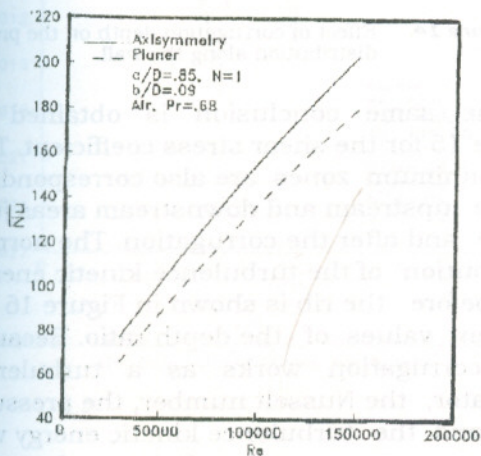
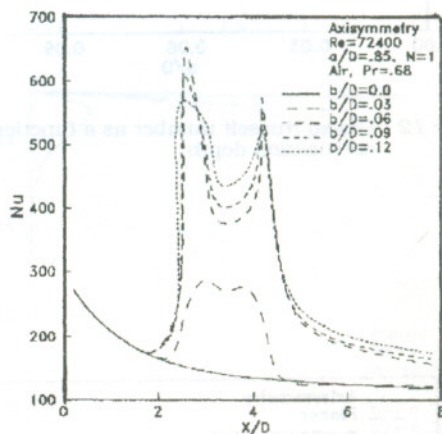


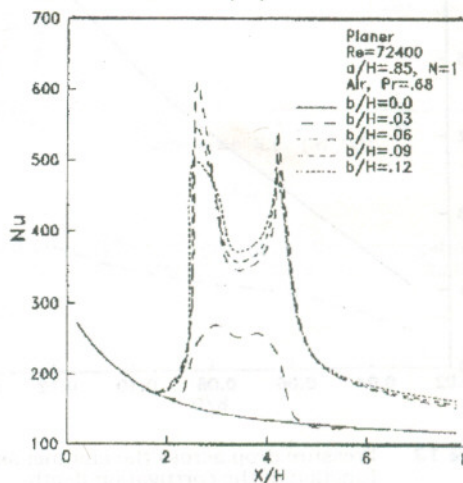
Figure 10 Effect of inlet Reynolds number on the global Nusselt number.

Effect of Corrugation Depth

As the reverse flow before and behind a corrugation leads to a sudden increase in the local Nusselt number, the deeper the corrugation, the greater the reverse flow zone which in turn increases the local and the global Nusselt number, as indicated in Figures 11 and 12 for different values of b/D (or b/H) from $b/D=0$ (case of flat duct) to 0.12 in both cases of axisymmetry and rectangular channels. On the other hand, when increasing the corrugation depth, the flow will be more blocked and the pressure loss across the step will be consequently increased, as seen from Figure 13. The static pressure along the wall decreases with increasing the corrugation depth, Figure 14.



(a)



(b)

Figure 11 Effect of corrugation depth on the local Nusselt number distribution.

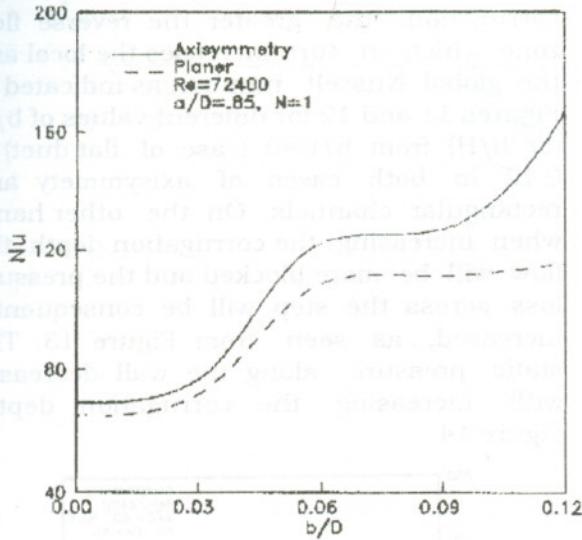


Figure 12 Global Nusselt number as a function of the corrugation depth.

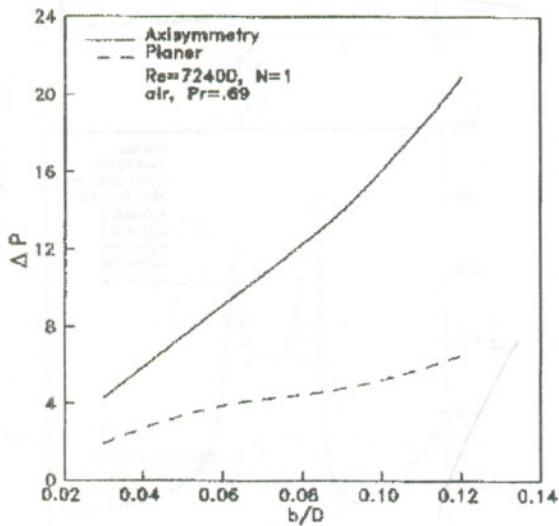
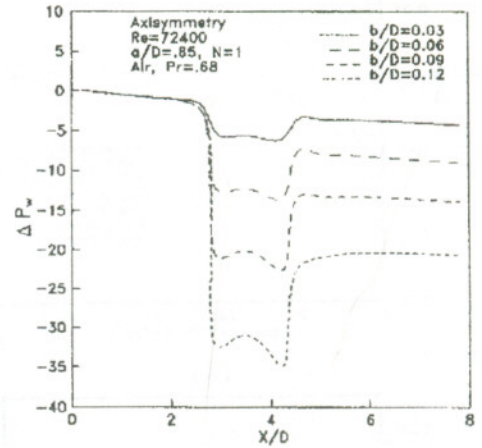
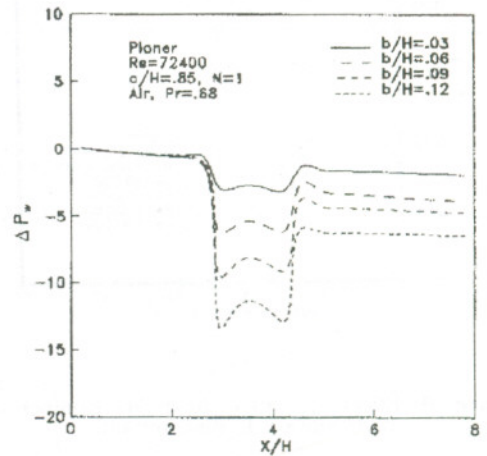


Figure 13 Pressure drop across the channel as a function of the corrugation depth.



(a)

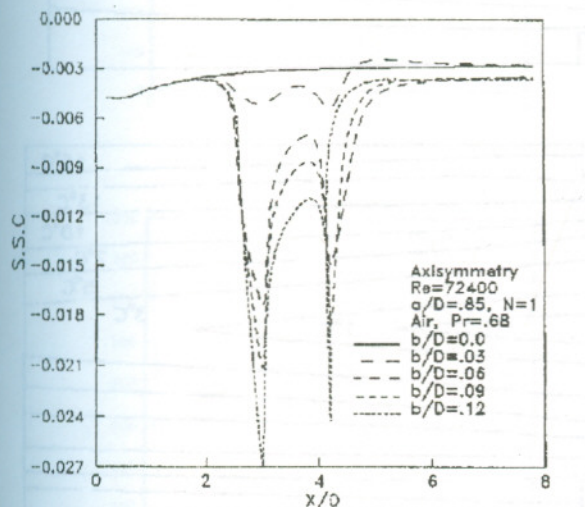


(b)

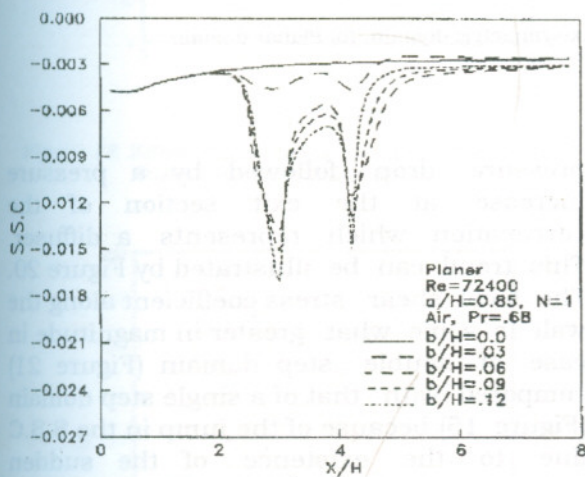
Figure 14 Effect of corrugation depth on the pressure distribution along the wall.

The same conclusion is obtained in Figure 15 for the shear stress coefficient. The two minimum zones are also corresponding to the upstream and downstream areas just before and after the corrugation. The normal distribution of the turbulence kinetic energy just before the rib is shown in Figure 16 for different values of the depth ratio. Because the corrugation works as a turbulence generator, the Nusselt number, the pressure drop and the turbulence kinetic energy will increase as a result of increasing the corrugation depth.

Figure 17 represents the temperature fields (isothermal lines) in case of circular as well as rectangular ducts having a single corrugation for values of inlet Reynolds number (72400), corrugation width ratio (0.85), depth ratio (0.09) and wall temperature (100 °C). The penetration of the thermal boundary layer inside the fluid can be easily seen from the figure.

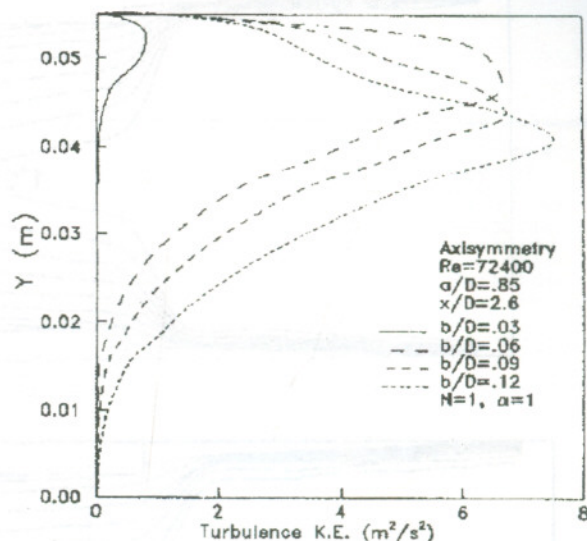


(a)

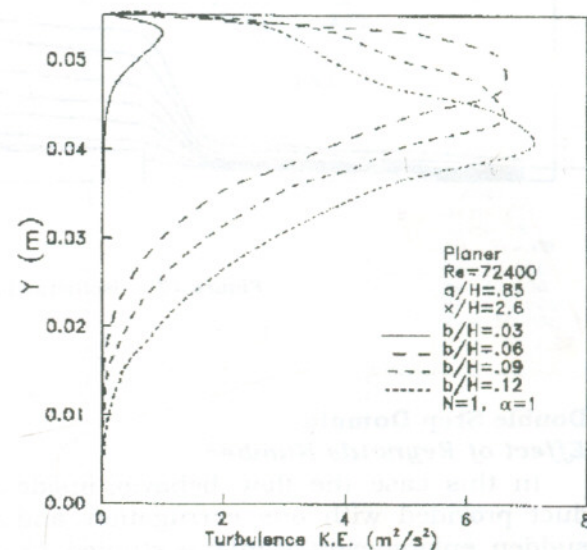


(b)

Figure 15 Effect of varying the corrugation depth on the local shear stress coefficient.



(a)



(b)

Figure 16 Effect of changing the corrugation depth on the turbulence K. E. distribution

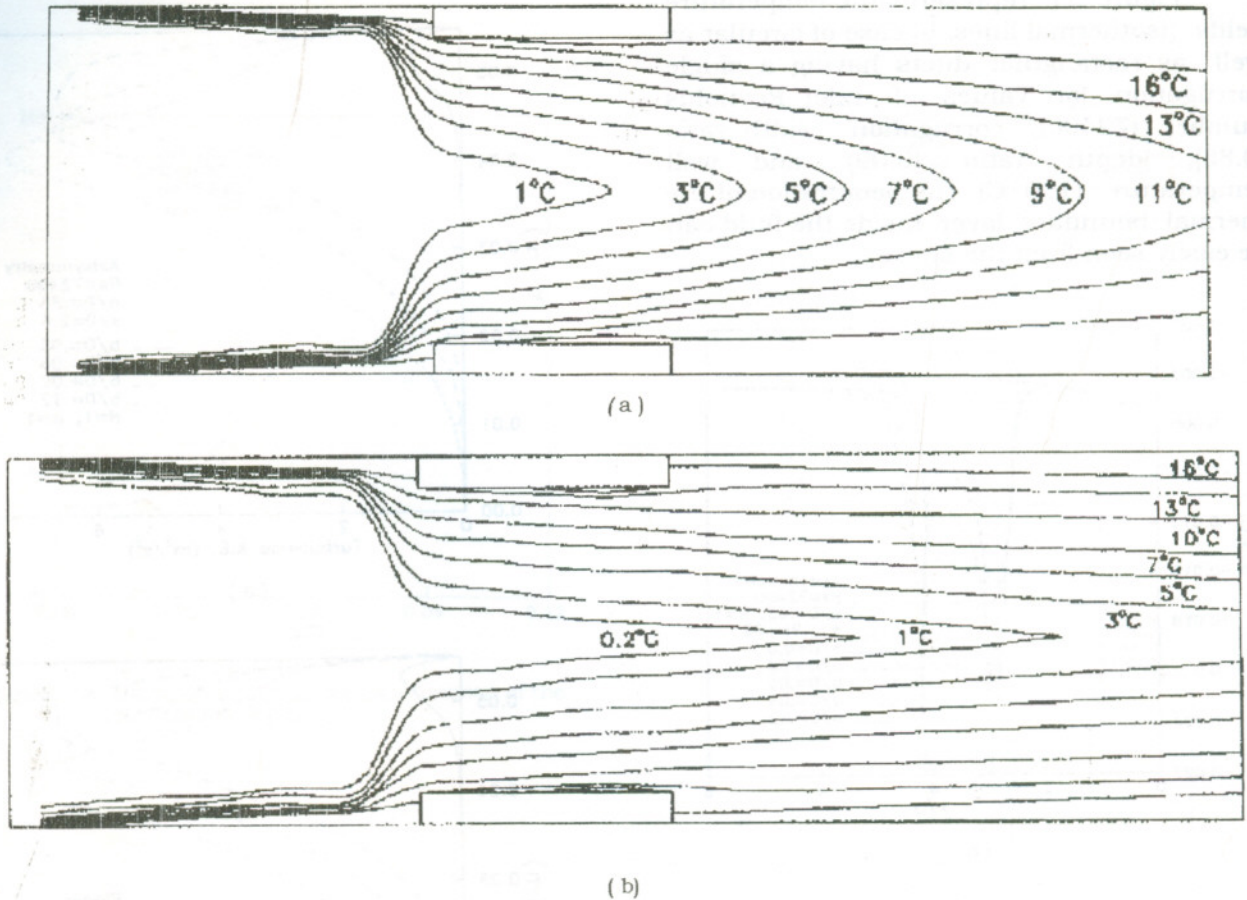


Figure 17 Isothermal lines: (a) Axisymmetric domain, (b) Planar domain.

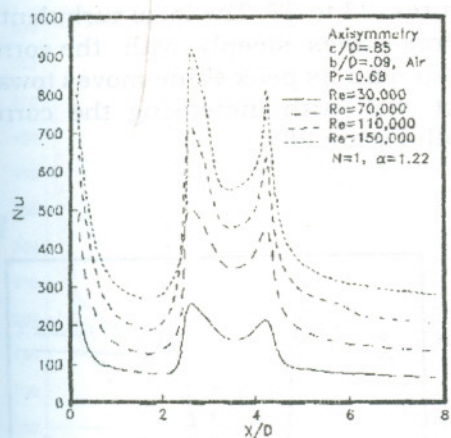
Double Step Domain Effect of Reynolds Number

In this case the flow behavior inside a duct provided with one corrugation and a sudden enlargement at inlet is studied. This configuration ensures three corners, a condition which leads to three corresponding peaks in the local Nusselt number distribution curves, as shown in Figure 18 and consequently a raise in the global Nusselt number (Figure 19).

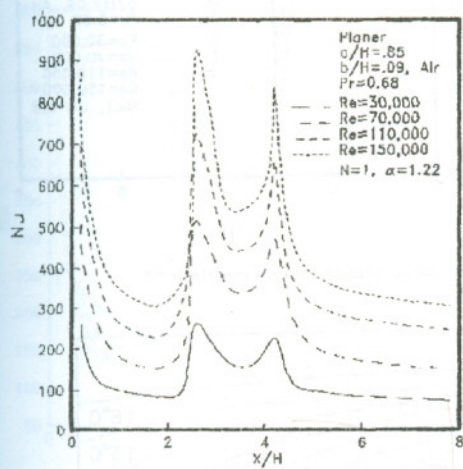
On the other hand, the sudden enlargement works as a diffuser which transforms the kinetic energy into enthalpy resulting in an increase of the static pressure downstream the sudden enlargement. Then, the inlet part of the corrugation works as a nozzle leading to a

pressure drop followed by a pressure increase at the exit section of the corrugation which represents a diffuser. This trend can be illustrated by Figure 20. The local shear stress coefficient along the wall is some what greater in magnitude in case of double step domain (Figure 21) compared with that of a single step domain (Figure 15) because of the jump in the S.S.C due to the existence of the sudden enlargement at inlet. Figure 22 explains the deeper penetration of the thermal boundary layer in the fluid in case of double step domain rather than that of a single step one Figure 17.

Simulation of Enhanced Turbulent Heat Transfer in Corrugated Wall-Channels

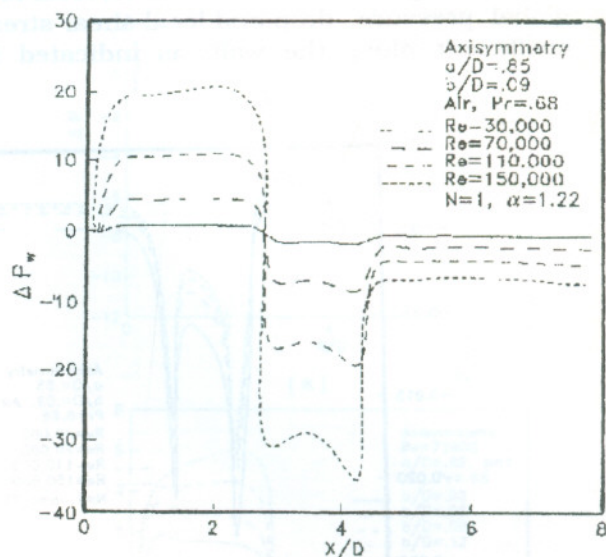


(a)

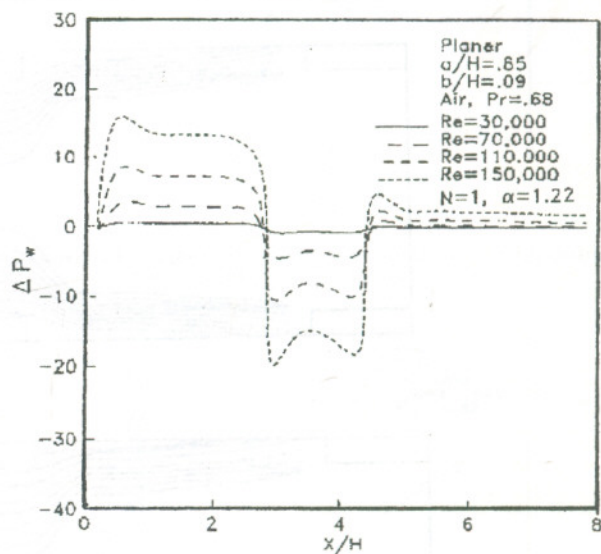


(b)

Figure 18 Effect of inlet Reynolds number on the local Nusselt number distribution.



(a)



(b)

Figure 20 Effect of inlet Reynolds number on the pressure distribution along the wall.

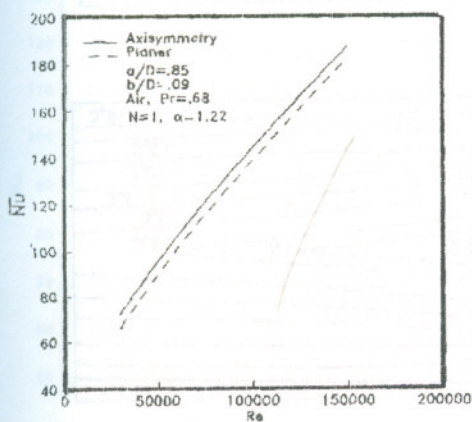


Figure 19 Global Nusselt number as a function of the inlet Reynolds number.

Effect of Corrugation Depth

The increase of the corrugation depth leads to a corresponding increase in the local and global Nusselt number, local and global pressure drop and local shear stress coefficient along the wall, as indicated in

Figures 23 to 27. The local turbulent kinetic energy varies steeply with the corrugation depth and its peak value moves towards the duct wall with increasing the corrugation depth Figure 28.

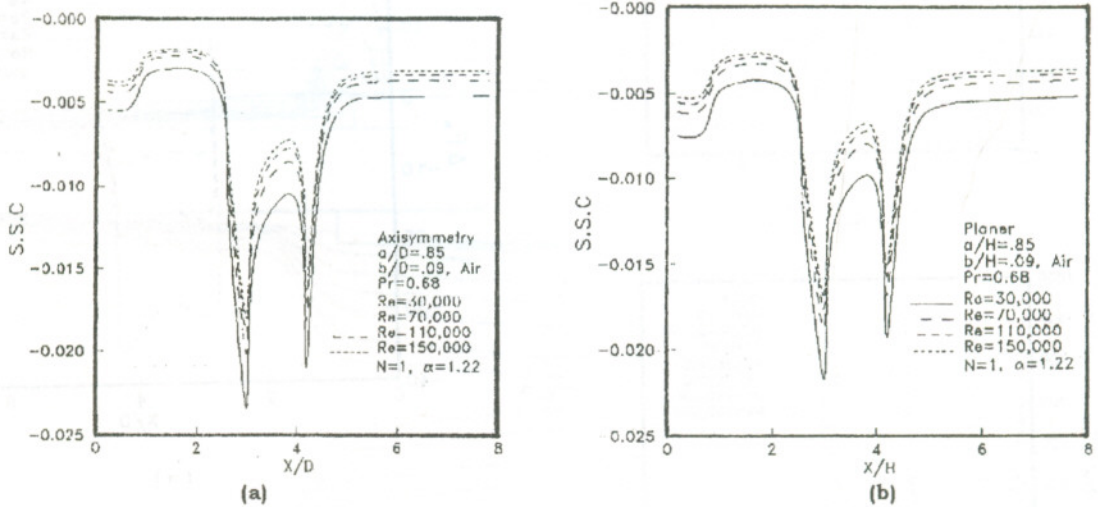


Figure 21 Effect of inlet Reynolds number on the local shear stress coefficient.

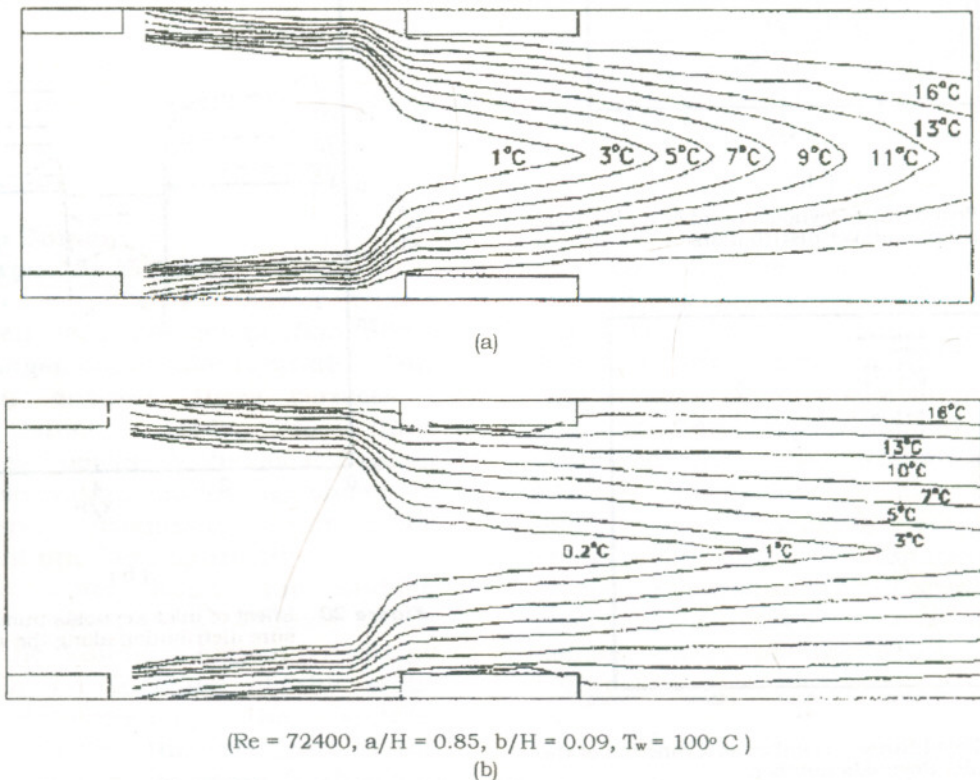
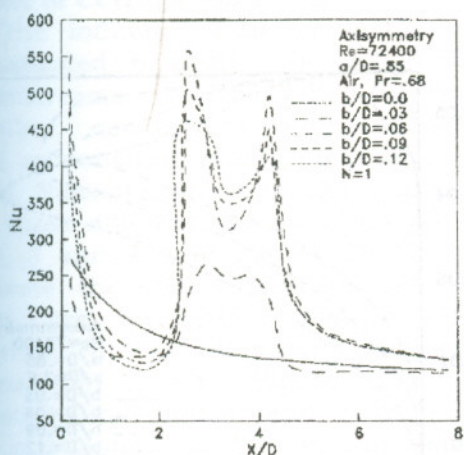
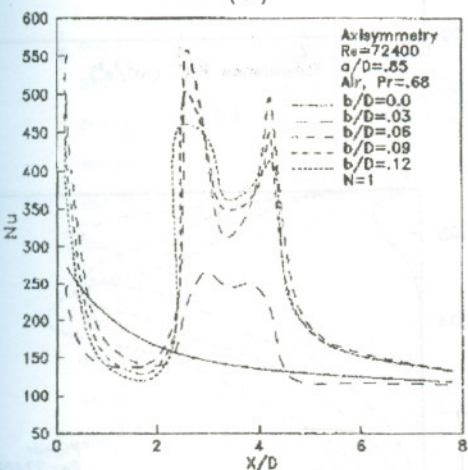


Figure 22 Isothermal lines: (a) Axisymmetric domain, (b) Planer domain.

Simulation of Enhanced Turbulent Heat Transfer in Corrugated Wall-Channels



(a)



(b)

Figure 23 Effect of corrugation on depth the local Nusselt number distribution.

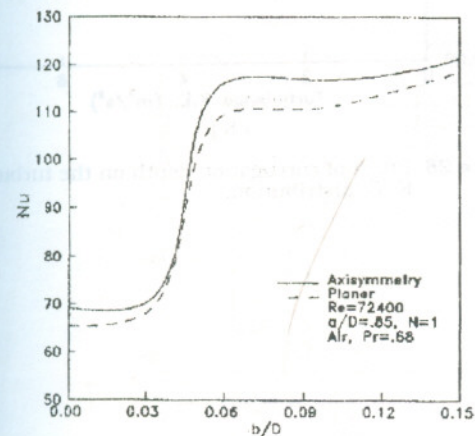
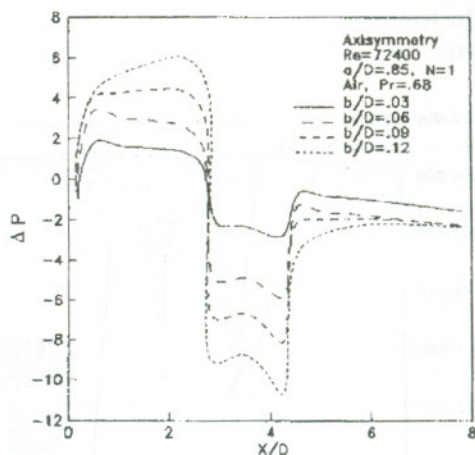
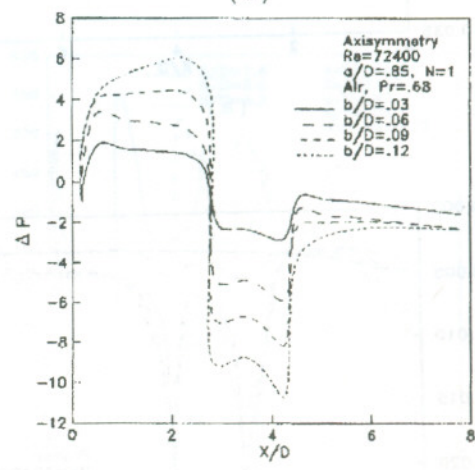


Figure 24 Global Nusselt number as a function of the corrugation depth.



(a)



(b)

Figure 25 Effect of corrugation depth on the pressure distribution along the wall.

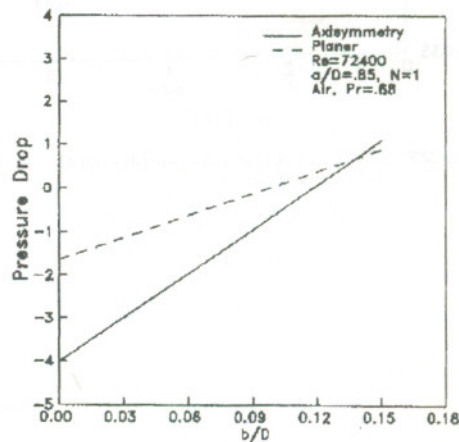
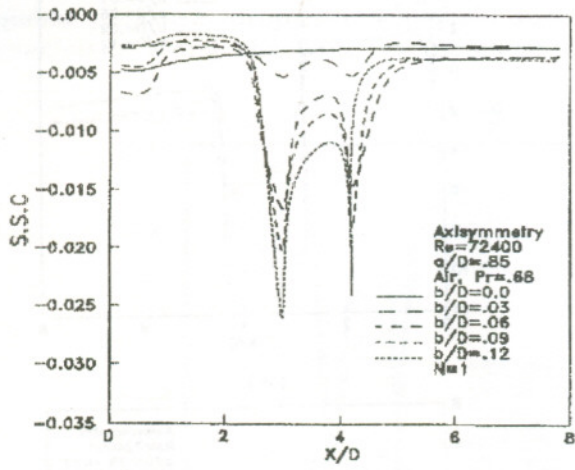
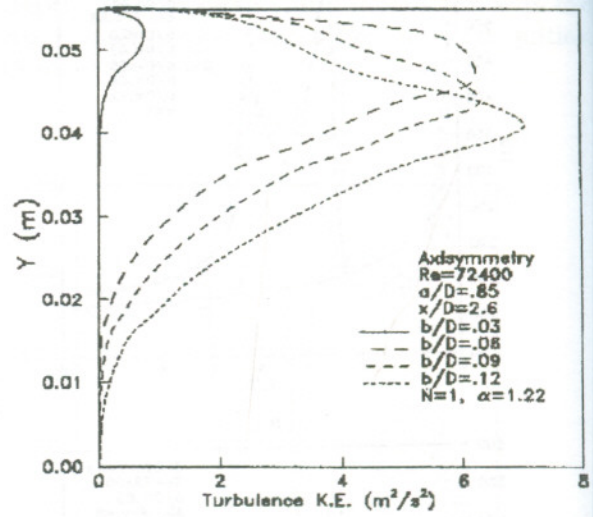


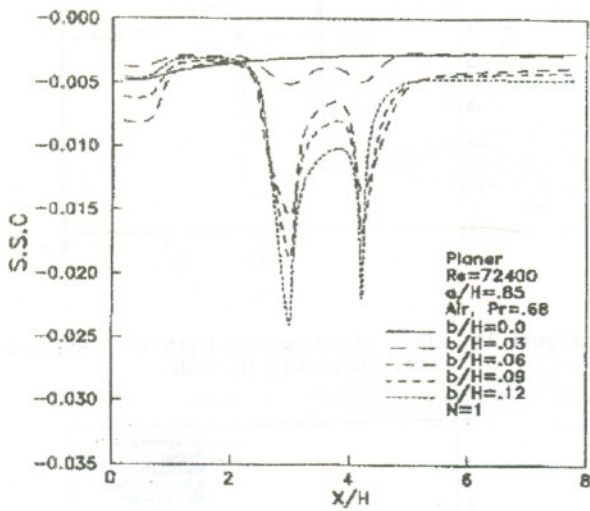
Figure 26 Pressure drop along the wall as a function of the corrugation depth.



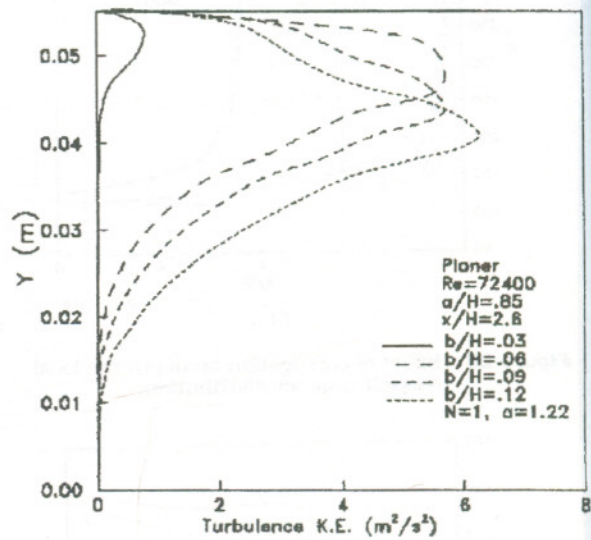
(a)



(a)



(b)



(b)

Figure 27 Effect of corrugation depth on the local shear stress coefficient.

Figure 28 Effect of corrugation depth on the turbulence K. E. distribution.

Effect of Corrugation Pitch

The influence of the corrugation pitch is investigated by shifting the second rib away downstreams at fixed values of Reynolds number, corrugation width and depth as well as constant enlargement ratio (α). The local Nusselt number distribution is plotted for three different values of the pitch ratio (1.8, 3 and 4.2) in Figure 29. These plots indicate the shift of the two peak values with the corrugation position and the decrease of their values with increasing the corrugation pitch. Figures 30 and 31 illustrate the diffuser and nozzle effects of the corrugation on the pressure drop and

the shear stress coefficient distribution respectively, and the displacement of their maximum and minimum values with the pitch ratio.

Figure 32 shows the velocity vector diagram inside a tube (Figure 32-a) as well as inside a rectangular channel (Figure 32-b) provided with two corrugations. The velocity vector diagrams are plotted at different locations for constant Reynolds number (72400) and a fixed value of corrugation depth ratio (0.21). The figure indicates the development of the flow along the corrugated channels.

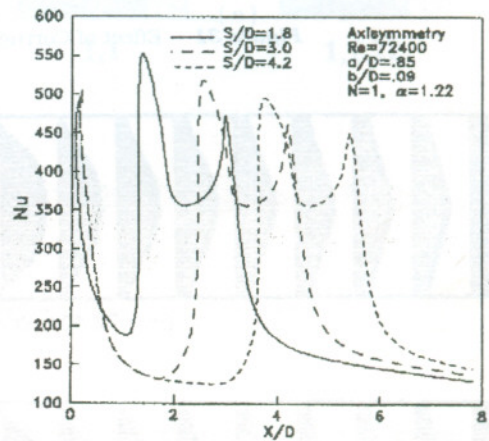
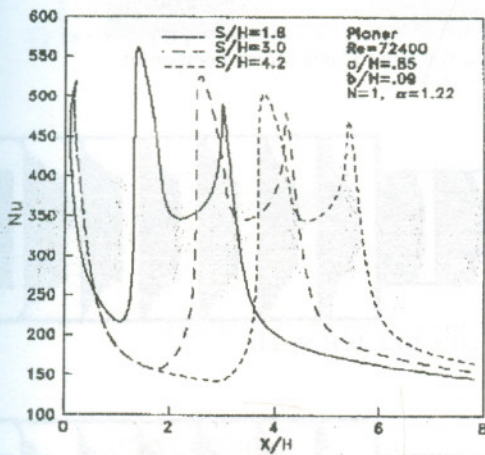


Figure 29 Effect of corrugation pitch on the local Nusselt number distribution.

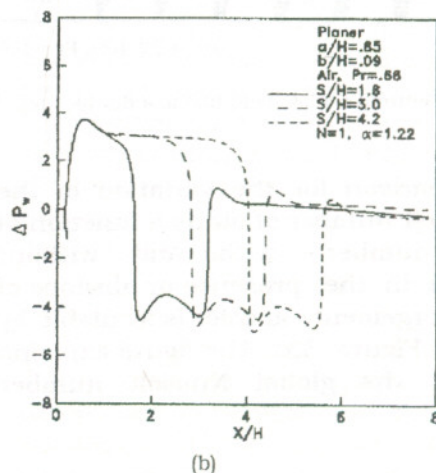
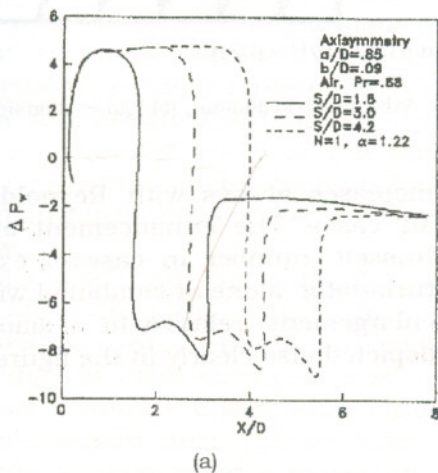
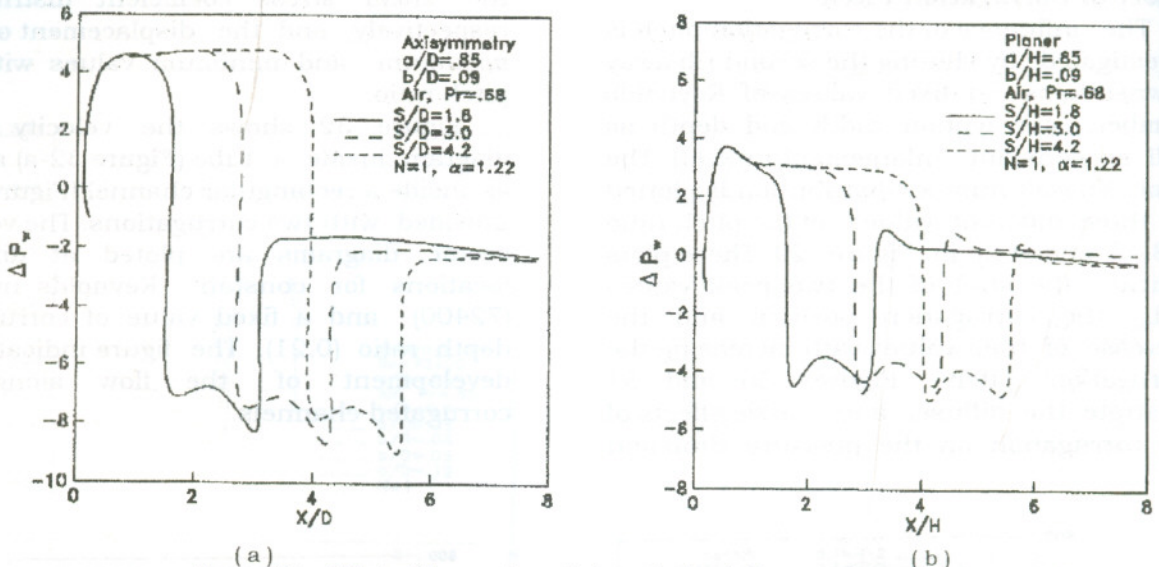
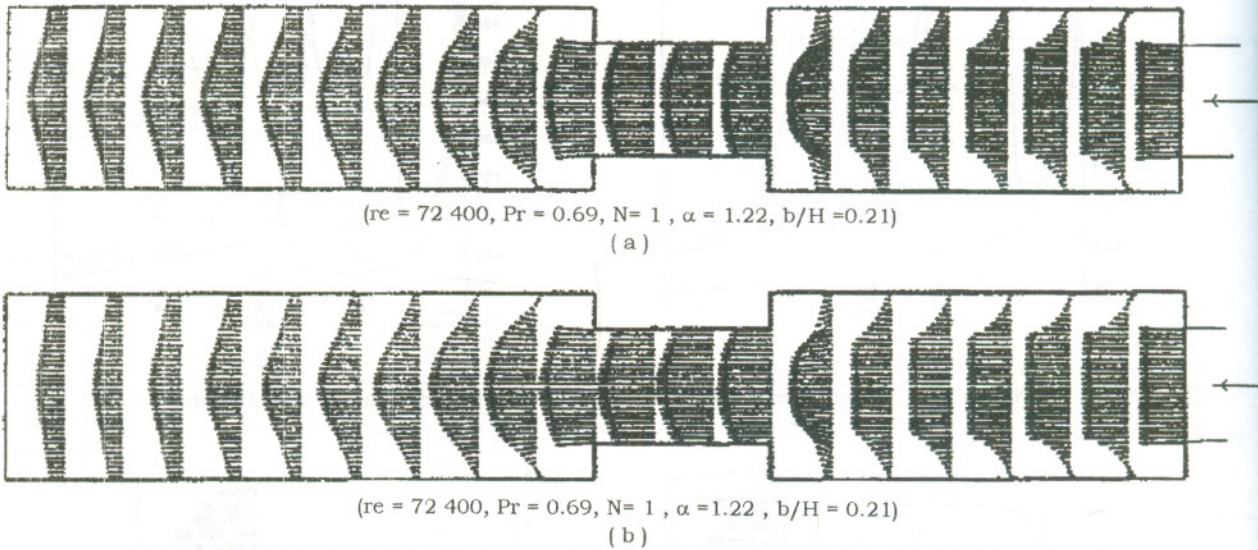


Figure 30 Effect of corrugation pitch on the pressure distribution along the wall.



(a) (b)
Figure 31 Effect of Corrugation pitch on the local shear stress coefficient.



(re = 72 400, Pr = 0.69, N = 1, $\alpha = 1.22$, b/H = 0.21)
 (a) (b)
Figure 32 Flow field inside a double step domain; (a) Axisymmetric domain, (b) Planer domain.

A comparison for the variation of the global Nusselt number of air as a function of Reynolds number with and without corrugations in the presence or absence of sudden enlargement at inlet is available by columns in Figure 33. The figure explains clearly that the global Nusselt number

increases always with Reynolds number in all cases. The enhancement of the global Nusselt number in case of existing a rib turbulator alone or combined with a sudden enlargement relative to a smooth duct is depicted also clearly in the figure.

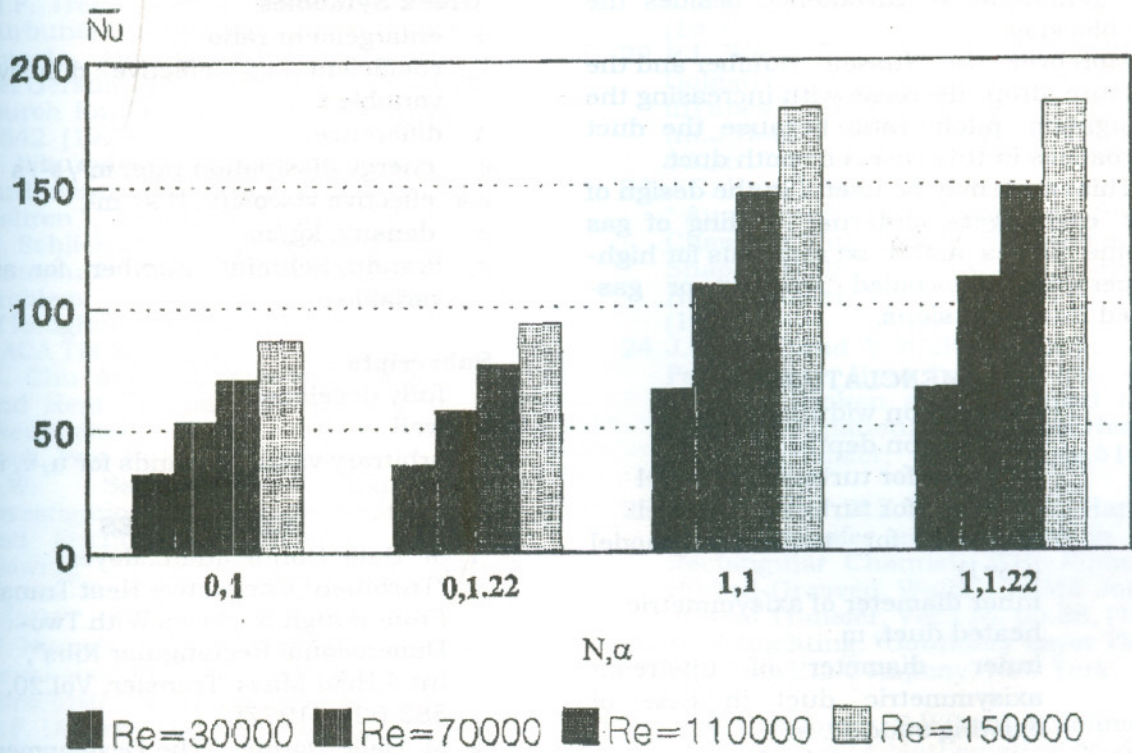


Figure 33 Variation of global Nusselt number with the channel geometry.

CONCLUSION

Heat transfer and pressure drop responds of a corrugated short duct are determined numerically for turbulent flow. Both circular and rectangular flow channels are taken into account. Computations are carried out for Prandtl number of 0.69 (air), in the Reynolds number range of 30000 to 150000 for four assigned corrugation depth ratios (0.03, 0.06, 0.09 and 0.12) and three values of corrugation pitch ratio (1.8, 3 and 4.2). The main conclusions of the results are given below:

Both the local and the global Nusselt number are increased due to the establishment of double peaks corresponding to each corrugation in the local Nusselt number distribution curves over that of a smooth duct. This tendency is owing to the generation of a reverse flow upstream and downstream the corrugation.

The enhancement in the average Nusselt number in case of circular ducts is higher than that in case of a rectangular ducts at the same corrugation width and depth ratios and under the same flow conditions because of the compactness property of the axisymmetric ducts. On the other hand, a steep pressure drop occurs across a corrugation which returns to the effect of flow separation behind and in front of the rib yielding two minimum zones in the static pressure distribution upstream and downstream the rib.

It is observed also that the Nusselt number and the pressure drop increase with both Reynolds number and the corrugation depth ratio. A corrugation works as a turbulence generator and this explains the enhancement of Nusselt number with increasing the corrugation depth ratio, while the increase in the pressure drop returns to

the generation of turbulence besides the flow blockage.

Moreover, the Nusselt number and the pressure drop decrease with increasing the corrugation pitch ratio because the duct approaches in this case a smooth duct.

This work may be useful in the design of heat exchangers, internal cooling of gas turbine blades and heat removals for high-temperature gas-cooled reactors or gas-cooled nuclear fusions.

NOMENCLATURE

| | |
|----------------|--|
| a | corrugation width, m |
| b | corrugation depth, m |
| C ₁ | constant for turbulence model |
| C ₂ | constant for turbulence model |
| C _D | constant for turbulence model (C _D =1) |
| D | inner diameter of axisymmetric heated duct, m |
| d | inner diameter of upstream axisymmetric duct in case of existing sudden, m |
| | enlargement at inlet |
| G | rate of generation of turbulence energy, m ² /s ² /s |
| H | height of downstream heated flat duct, m |
| h | convective heat transfer film coefficient, W/m ² K |
| i | specific enthalpy, J/kg |
| k | turbulence kinetic energy, m ² /s ² |
| N | number of corrugations |
| Nu | Nusselt number |
| Pr | Prandtl number |
| p | pressure, Pa |
| R | distance between the channel centerline and the wall, m |
| Re | Reynolds number |
| S | corrugation pitch, m |
| S.S.C | shear stress coefficient |
| S _r | arbitrary source term of the conservation equation |
| u | axial velocity component, m/s |
| v | velocity component normal to the wall, m/s |
| x | axial coordinate, m |
| y | distance normal to the duct wall, m/s |

Greek Symbols

| | |
|-----------------|--|
| α | enlargement ratio |
| Γ_{ϕ} | coefficient of effective diffusivity for variable ϕ |
| Δ | difference |
| ϵ | energy dissipation rate, m ² /s ² /s |
| μ_{eff} | effective viscosity, N.s/ m ² |
| ρ | density, kg/m ³ |
| σ_{ϕ} | Prandtl/Schmidt number for arbitrary variable ϕ |

Subscripts

| | |
|--------|--|
| f | fully developed |
| w | wall |
| ϕ | arbitrary variable stands for u, v, i, k, ϵ |

REFERENCES

1. M. Dalle Donne and L.Meyer, "Turbulent Convective Heat Transfer From Rough Surfaces With Two-Dimensional Rectangular Ribs", Int.J.Heat Mass Transfer, Vol.20, pp. 583-620. (1977)
2. M. Dalle Donne, "The Development of the Gas Cooled Fast Breeder Reactor", in beitrage zur kerntechnik, karl wirtz, gewidmet zum 65. Geburtstag, KFK 2200 (1975).
3. G. Melese D'Hospital, "Merit Index for Gas-Cooled Reactor Heat Transfer", Nucl.Sci.Engng, Vol.50, pp.83-85. (1973)
4. Tong-Miin Liou and Jenn-Jiang Hwang, "Effect of Ridge Shapes on Turbulent Heat Transfer and Friction in Rectangular Channel", Int.J.Heat Mass Transfer, Vol. 36, pp.931-940. (1993)
5. L. Schiller, "Uber den Stromungswiderstand von Rohren verschiedenen Querschnitts und Rauigkeitsgrades", z.Angew. Math.Mech,3, (1923).
6. L. Hopf, "Die Messung der Hydraulischen Rauigkeit", z.Angew. Math.Mech.3, (1923).
7. K.Fromm, "Stromungswiderstand in Rauhen Rohern", z.Angew. Math.Mech.3, (1923).
8. A.H. Gibson, "The Flow of Water in a Corrugated Pipe", Phil.Mag. Vol. 50, pp. 199-204. (1925)
9. W. Fritsch, "Der Einflub der Wandrauigkeit auf Turbulente Geschwind- Igketsverteilung in Rinnen", Angew. Math.Mech, 8, (1928).

- M.F. Treer, "Der Widerstandsbeiwert bei Turbunte Strömungen Durch Rauhe Kanäle. Die Geschwin Keitsverteilung bei Geradlinigen Turbulenten Stromun Durch Rauhe Kanäle", *Phys.z*, 9, pp. 538 - 542. (1929).
11. S. Nikuradse, "Gesetzmabigkeiten der Turbulente Stromung in Glatten Rohren ", *ForschHft.Ver.Dt.*, (1932).
 12. H. Schlichting, " Experimentelle Untersuchungen zur Rauhgkeits Problem (Experimental Investigation of Roughness Problem)", *Ing.-Arch.*7(1), NACA TM 823, pp.1-34. (1937)
 13. H. Chu and V.L.Streeter, " Fluid Flow and Heat Ttransfer in Artificially Roughened Pipes", *Illinois Inst. of Tech.,Proc.No.4918*, (1949).
 14. E.W. Sams, " Experimental Investigation of Average Heat Transfer and Friction Coefficients For Air Flowing in Circular Tubes Having Square-Thread-Type Roughness", NACA, E52D17, (1952).
 15. W. Nunner, " WarmeUbergang und Druckabfall in Rauhern Rohren ", *ForschHft.Ver.Dt.Ing.*455, (1956).
 16. D.F. Dipprey and D.H.Sabersky, " Heat and Momentum Transfer in Smooth and Rough Tubes at Various Prandtl Numbers", *Int.J.Heat Transfer* 6, (1963)
 17. E.D. Brouillette, T.L.Mefflin and J.E. Myers, " Heat Transfer and Pressure Drop Characteristics at Internal Finned Tubes", ASME Paper 57-A-47, (1957).
 18. R. Koch, " Pressure Loss and Heat Transfer For Turbulent Flow", AEC-Tr-3875, (1960).
 19. J. Molloy, " Rough Tube Factors and Heat-Transfer Coefficients in Laminar and Transition Flow", UKAEA AERE-R5415, (1967).
 20. J.Gargaud and G.Paumard, "Ameloration du Transfert de Chaleur par Emploi de Surfaces Corrugées", Commissariat a L'energy Atomique, Report CEA-2464, (1969).
 21. E.K. Kalinin, G.A.Dreistler and S.A. Yarkho, " Augmentation of Connective Heat and Mass Transfer", A.E.Bergles and R.L.Webb (Eds.) ASME, New York, (1970).
 22. R.L. Webb, E.R.G.Eckert and R.J. Goldstein, " Heat Transfer and Friction inTubes With Repeated-Rib Roughness", *Int.J.Heat Mass Transfer* Vol. 14, pp. 601-617. (1971)
 23. J.C. Han, Y.M.Zhang and C.P.Lee, " Augmented Heat Transfer in Square Channels With Parallel, Crossed and V Shaped Angled Ribs", *ASME Journal of Heat Transfer*, Vol.113, pp. 590-596. (1991)
 24. J.C. Han and Y.M.Zhang, " High Performance Heat Transfer Ducts With Parallel Broken and V-Shaped Broken Ribs", *International Journal of Heat and Mass Transfer*, Vol.35, pp.513-523. (1992)
 25. Y.M. Zhang, W.Z.Gu and J.C.Han, " Heat Transfer and Friction in Rectangular Channels With Ribbed or Ribbed-Grooved Walls", *ASME Journal of Heat Transfer*, Vol.116, pp.58, (1994)
 26. H. Schlichting, "Boundary Layer Theory", Mc-GrawHill Company, New York, (1968).
 27. M.K. Bassiouny, S.Wilson, S.Soliman and Y.Rihan, "A Mathematical Model For Simulating the Flow Pattern and Local Heat Transfer Coefficient in Ducts With Sudden Enlargement", *Alexandria Engineering Journal*, Vol.35, No.1, pp.A-21-36. (1997)
 28. S.V. Patankar, "Numerical Heat Transfer and Fluid Flow", Hemisphere Publishing Corporation, (1980).
 29. T.M. Lio and J.J.Hwang, " Effect of Ridge Shapes on Turbulent Heat Transfer and Friction in a Rectangular Channel", *Int.J.Heat Mass Transfer*, Vol.36, No.4, pp.931-940, (1993)
 30. T.M.Lio and J.J.Hwang, " Turbulent Heat transfer Augmentation and Friction in Periodic Fully Developed Channel Flows", *ASME J.Heat Transfer* Vol.114, pp.56-64, (1992).

Received February 26, 1998
Accepted March 31, 1998

محاكاة انتقال الحرارة للسريان المضطرب فى القنوات ذات الألواح المعرجة

محمد خليل بسيونى* ، صفوت ولسن* ، صلاح الدين سليمان** ياسر ريحان**

* قسم هندسة القوى الميكانيكية - جامعة المنوفية

** مركز المعامل الحاره - هيئة الطاقة الذرية

ملخص البحث

تم عمل نموذج رياضى لدراسة الخصائص الهيدوديناميكية وانتقال الحرارة للسريان الاضطرابى فى القنوات القصيرة ذات الألواح المعرجة . وتم استخدام نموذج الاضطراب $k-\epsilon$ فى برمجة السريان مع عمق تعريجات 0.3 , الى 1.2 , ونسبة الخطوة 1.8 و 3 و 4.2 . وكان رقم رينولدز يتراوح بين 30000 و 150000 . وأعتمد النموذج الرياضى على معادلات بقاء الكتلة والعزم والطاقة . وتم حل هذه المعادلات معا باستخدام طريقة محلل الحجم الدقيق . وتم عرض توزيعات رقم نسلت للهواء وتوزيعات الضغوط على الجدران واجهادات القص والطاقة الاضطرابية . وهناك عدة مقارنات مع نتائج عملياته سابقة لباحثين مختلفين وأوضحت المقارنات توافق كبير مع هذه النتائج . ويمكن استخدام هذه النتائج فى تصميم ريش التوربينات الغازية المبردة داخليا أو المفاعلات المبردة بالغاز .